Efficient analysis of arrays of compact metallic elements devoted to satellite SAR

Thomas Pairon[1], Sumit Karki[1], Stefania Monni[2], Christophe Craeye[1]
[1]Université catholique de Louvain: ICTEAM Institute, Antenna Group, Louvain-la-Neuve, Belgium,
thomas.pairon@uclouvain.be
[2]Netherlands Organisation for Applied Scientific Research: The Hague, The Netherlands, stefania.monni@tno.nl

***Abstract*—A fully metallic monopole element is proposed for satellite SAR antennas. This element has significant gain in the broadside direction thanks to its curved arm. This element is then studied in a large sparse array. A fast analysis technique is presented in order to solve for the currents of few hundreds elements, which correspond approximately to one millon basis functions. This method is based on macro basis functions coupled with an iterative solver accelerated with a multipole decomposion. This combination reduces drastically the memory requirements and shrinks the execution time. Good comparison between the proposed method and a commercial software solution is provided.**

***Index Terms*—monopole antenna, circular polarization, multipole, macro basis function, domain decomposition.**

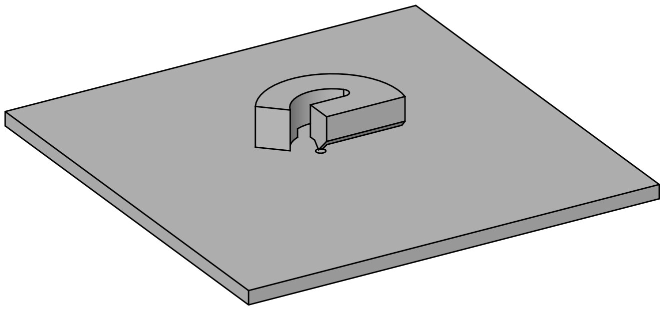

Fig. 1: Curved monopole element on a ground plane.

I. Introduction

Synthetic aperture radar (SAR) making use of arrays allows better cross-track resolution [1], [2]. The power involved in transmitting SAR antennas can be very high, and temperature variations for satellite-based antennas are typically large. The use of metallic radiating elements can alleviate both problems. However, it is not easy to find purely metallic elements with patterns as wide and smooth as those of antennas printed on dielectric material. This challenge becomes more critical when significant bandwidth is required.

The goal of this paper consists in proposing a fully metallic element with a relative frequency band in the order of 3 %, suitable for typical SAR applications [3], and a technique that allows dealing efficiently with the effects of mutual coupling between those elements, through an integral-equation solver. Regarding the choice of the element, it is compatible with basic pattern requirements for SAR in terms of beamwidth [4] and axial ratio. Leverage is found in the limited scan range of SAR antennas onboard satellites [3]. This means that elements with substantial gain can be used, i.e. of the order of 8 or 9 dB, as compared with 6 or 7 dB for microstrip antennas. Indeed, if the angular domain over which the array is scanned is itself located well within the main beam of the element pattern, the array pattern will not be specifically affected by the variation in the element pattern. On the contrary, to a certain extent, the higher gain of the element in the region of scan may improve the link budget and help suppress the sidelobes. In this endeavor, it is necessary to take into account the variation of the ("embedded") element patterns within the array as a result of mutual coupling [5]. Since this effect may impact the array pattern while it is scanned, it is important to be able to predict it accurately and efficiently. This will be carried out here using the Method of Moments (MoM), accelerated with a combination of Macro Basis Function (MBF) [6] representations and Fast Multipole Method (FMM). In a nutshell, the method will be made iterative, while limiting dramatically the number of radiation patterns that need to be computed in the traditional FMM approach [7].

The remainder of this paper is organized as follows. Section II shows the proposed element and Section III details the analysis technique and provides numerical results. Section IV concludes with comments on the timing and memory requirements of the proposed method and perspectives for improvement.

II. Antenna Element

The antenna element is shown in Fig. 1 atop a ground plane. The antenna is a monopole that is strongly curved and aligned horizontally to the ground plane so as to radiate in the broadside direction. The tip of the monopole is grounded to drain the horizontal current, which helps to improve the circular polarization purity, and also to improve mechanical support. The element can be fed with an SMA connector directly in the center. This is represented here with a delta-gap source.

A. Design

The array of the curved monopole elements would require a common ground plane. Because of the common ground plane,

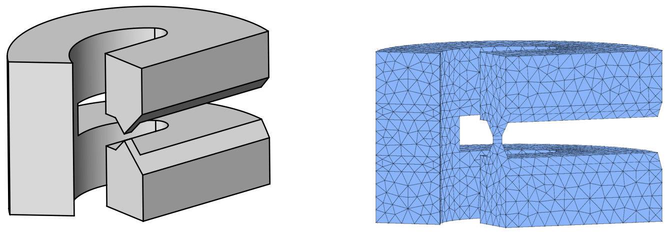

(a) (b)

Fig. 2: Equivalent dipole element. (a): perspective view, (b): mesh view.

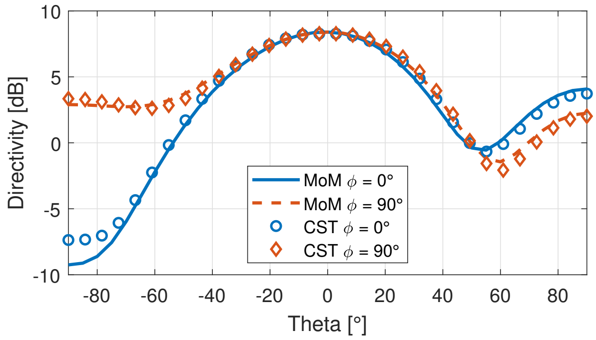

Fig. 4: Comparison of the element directivity computed with CST and UCLouvain's MoM code.

the array elements are not entirely disconnected. However, if we assume an infinite ground plane, the monopole element can be replaced by an equivalent dipole element as shown in Fig. 2.a. This would greatly improve the analysis speed at no extra cost to accuracy. The element is meshed with 5469 Rao-Wilton-Glisson (RWG) basis functions [8], as seen in Fig. 2.b.

B. Performance

Fig. 3 compares the reflection coefficient (S_{11}) at the input of the studied element, computed with CST Microwave Studio® and the MoM code developed at UCLouvain. One can observe that the MoM results are in good agreement with CST. The -15 dB impedance bandwidth of the antenna is 16%. Fig. 4 shows the directivity of the single element in the $\phi = 0$ and $\phi = \pi/2$ cuts. The element radiates at broadside with a 30° half-power beamwidth and a directivity of 8.4 dB. Again, the comparison between MoM and CST results is very good.

The axial ratio at broadside computed with CST is 3.9dB, while the UCLouvain MoM codes gives 3.7 dB. Those values are also in good agreement. Further optimization of the element would lead to axial ratio lower than 3 dB.

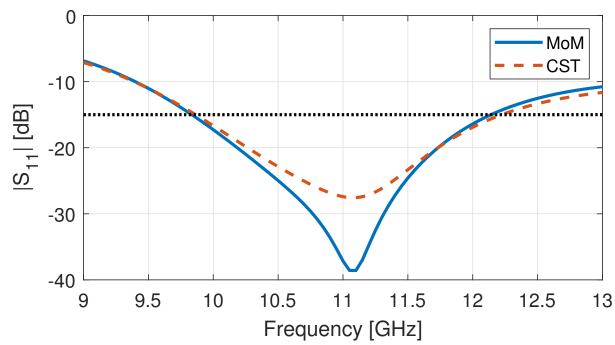

Fig. 3: Comparison of the reflection coefficient computed with CST and UCLouvain's MoM code. The black dotted line represents the -15 dB limit.

III. Combined MBF-multipole iterative solver

Solving large electromagnetic problems can be performed through iterative techniques, such as the Generalized Minimal Residual Method (GMRES) [9]. The solution is then approximated by a vector which belongs to a Krylov subspace. At each iteration, a matrix-vector product is performed, which offers a lower complexity compared to a matrix inversion. Faster convergence is reached when the current solution is expressed as a linear combination of Macro Basis Functions (MBFs). This approach goes well with iterative techniques, since the MBFs can be selected as portions of each generating vector computed at each new iteration [10]. The computational time of this approach is further reduced through the multipole expansion of the Green's function, which offers an efficient way to perform the matrix-vector product at each iteration [11]. Moreover, the multipole expansion also reduces the memory requirements, especially when the array is composed of identical elements. In that case, only one pattern is precomputed and stored for all the elements.

A. Solving for the currents via GMRES-MBF

Consider an array of M elements, each of them being described by N basis functions. The Electric Field Integral Equation (EFIE) can be solved via the Method of Moments (MoM), which consist in solving for $\mathbf{x}$ the following linear system of equations :

$$\mathbf{A}\mathbf{x} = \mathbf{b}, \tag{1}$$

where $\mathbf{A}$ is a $(MN \times MN)$ *impedance matrix*, which contains the reactions between all basis and testing functions over the domain, $\mathbf{x}$ is the currents vector of size $(MN \times 1)$ and $\mathbf{b}$ is the excitation vector of size $(MN \times 1)$.

The MBF approach rewrites each of the M^2 blocks of matrix $\mathbf{A}$ and each of the M segments of vector $\mathbf{b}$ in (1) as :

$$\begin{aligned} \mathbf{A}'_{i,j} &= \mathbf{K}^H \mathbf{A}_{i,j} \mathbf{K}, \\ \mathbf{b}'_i &= \mathbf{K}^H \mathbf{b}_i, \end{aligned} \tag{2}$$

where $\mathbf{K}$ is the set of MBFs, and $i, j \in [1 \ldots N]$ are the indices of the subdomains.

Since all the elements composing the array are the same, it is assumed that the set of MBFs is identical for all elements. Under this assumption, at each iteration, the new generating vector is split between all the elements, which corresponds to a $N \times M$ matrix . The P eigenvectors associated to the P highest singular values of this matrix are kept and form the $\mathbf{K}$ matrix of size $(N \times P)$.

The coefficients $\mathbf{I}$ of the MBFs for each elements are then computed by solving for $\mathbf{I}$:

$$\mathbf{A}'\mathbf{I} = \mathbf{b}'. \tag{3}$$

It is important to note that, since $P \ll N$, $\mathbf{A}'$ has a limited size of $(MP \times MP)$. $\mathbf{A}'$ easily fits in memory and (3) is easier to solve than the initial problem (1), even for very large problems. Indeed, the required memory is reduced by a factor $(N/P)^2$.

The solution is finally updated for each i element as :

$$\tilde{\mathbf{x}}_i = \mathbf{K}\mathbf{I}_i. \tag{4}$$

This process is made iterative as follows : at iteration $n+1$, the previous set of MBFs of the iteration n is discarded. A new set of MBFs is computed from the new generating vector obtained in a classical Krylov process. This is equivalent to a classical GMRES with a restart at each iteration. In other words, the generating vector at the $(n+1)^{\text{th}}$ iteration is equal to $\mathbf{b} - \mathbf{Z}\tilde{\mathbf{x}}^n$, where $\tilde{\mathbf{x}}^n$ contains all the segments $\tilde{\mathbf{x}}_i$ defined by (4). This slightly increases the number of required iterations [12], but the size of the system of equations (3) is kept constant, which offers good performance in terms of storage and computation time. For smaller problems, the set of MBFs can be augmented at each iteration [13]. This increases the size of $\mathbf{A}'$ at each iteration, which is not suitable for very large array as considered here in this paper.

B. Multipole fast matrix-vector product

The computation of the generating vector and the generation of MBFs involve matrix-vector products of relatively big matrices at each iteration. This is efficiently performed thanks to the multipole expansion of the Green's function. Each block $\mathbf{A}_{i,j}$ is expressed as :

$$\mathbf{A}_{i,j} = \mathbf{p}_i^*(\rho_i)\mathbf{T}(|\rho_i - \rho_j|)\mathbf{p}_j(\rho_j), \tag{5}$$

where $\rho_{i,j}$ is the central position of element i, j, $\mathbf{p}$ are the patterns for all the basis functions computed in only a few directions and $\mathbf{T}$ is the translation diagonal matrix (stored as a vector). Note that since the elements are identical and support identical MBFs, only one set $\mathbf{p}$ of P patterns needs to be computed for all the N elements. Regarding the self interacting blocks $\mathbf{A}_{i,i}$ which are all identical, so that they are computed only once and stored in memory.

When computing the generating vector, each pattern $\mathbf{p}_j$ can be multiplied in advance at each iteration with the corresponding input segment. This result is then multiplied element-wise with each component of the diagonal in matrix $\mathbf{T}$. Regarding the matrix-vector multiplication of (2), $\mathbf{K}^H\mathbf{p}^*$ and $\mathbf{K}\mathbf{p}$ are precomputed. Moreover, since $\mathbf{K}$ is the same for all elements, those products are computed only once at each iteration. This is where the use of identical MBFs on all elements brings an important advantage when combined with a multipole process.

The multipole expansion coupled with identical elements dramatically reduces the computational time as well as the memory requirements in the proposed iterative scheme (see Sec. IV for numerical values).

IV. Numerical Results

A. Validation of the iterative MBF solver

The proposed iterative scheme is validated with respect to a brute-force approach on an array of 4 elements. In this case, none of the blocks of the matrix is compressed with multipoles. The current associated to each basis function is compared for both methods and is numerically the same, as depicted on Fig. 5.

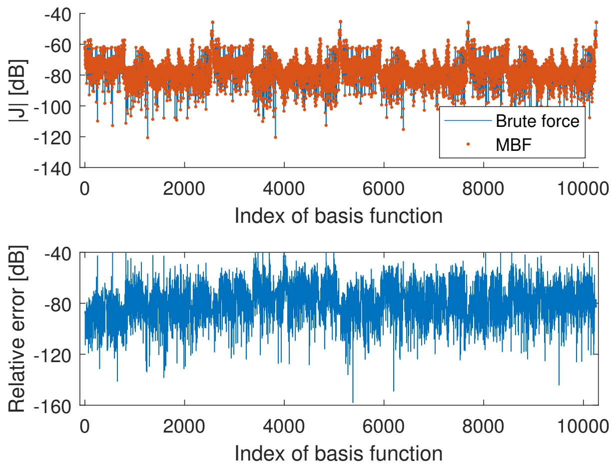

Fig. 5: Validation of the MBF method versus brute force for a 4 elements array. On the top figure, plain black line corresponds to the brute force solution; gray dots represents the currents computed with the MBF approach.

B. Study of sparse 512-elements array

A sparse array composed of 512 elements is analyzed, with each element described with 5469 RWG basis functions. The total number of basis functions of the array is 2,800,128. The positions of the antennas are depicted on Fig. 6, with a minimal distance between two neighbouring elements of 1.39λ. Elements are randomly iteratively distributed one by one in a given area, under the constraint of minimal distance between elements. Given this minimal distance, the near-interaction matrix only contains the self impedance diagonal terms; all the other subdomains interactions are accelerated using the multipole decomposition described in (5). This further reduces the computational time and the required memory space.

The normalized radiation pattern is illustrated on Fig. 7 for a constant phase excitation at each element. One can observe on Fig. 7 that with constant phase, the maximum of directivity is located at broadside. The first sidelobe has an amplitude of -12.7 dB and is located at $\pm 0.9°$. First sidelobe can be further reduced by applying amplitude tapering on each element. The axial ratio at broadside is 4.3dB.

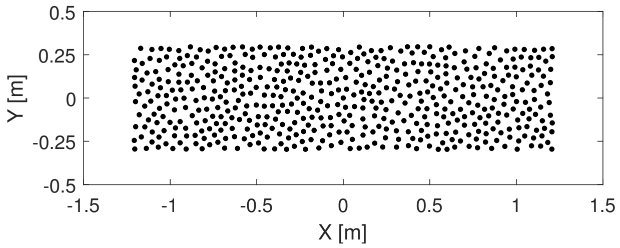

Fig. 6: Positions of the 512 elements of the array

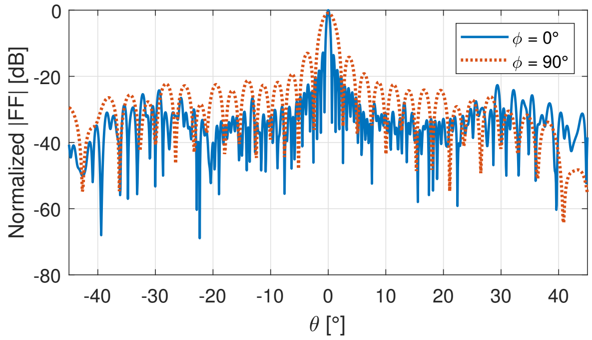

Fig. 7: Normalized far field radiation pattern for $\theta \in [-45; 45]^\circ$ for uniform phase excitation.

On Fig. 8, the beam is steered in the direction $(\theta, \phi) = (-22.5, 0)^\circ$ with phase shifts applied correspondingly at each antenna. Thus, it is possible to steer the beam around broadside incidence without impacting significantly the level of the sidelobes. The axial ratio at $(\theta, \phi) = (-22.5, 0)^\circ$ is equal to 4.4dB.

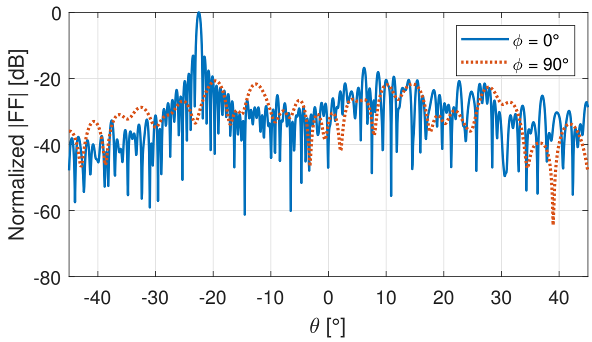

Fig. 8: Normalized far field radiation pattern for $\theta \in [-45; 45]^\circ$ steered to the direction $(\theta, \phi) = (-22.5, 0)^\circ$.

C. Memory and computation time

The convergence of the solution, represented by the norm of the GMRES residue, is illustrated on Fig. 9. A fixed number of MBFs is kept at each iteration, i.e. the size of $\mathbf{K}$ is fixed by a chosen parameter. In this example, 10, 20 and 30 MBFs are selected.

TABLE I: Timing required with respect to the number of MBFs.

	10 MBFs	20 MBFs	30 MBFs
tPrep	19m51s	19m51s	19m51s
tProduct	19s	19s	19s
tFill	34s	1m1s	1m57s
tSolving	3s	25s	1m21s
tTotal	61m6s	48m45s	55m15s

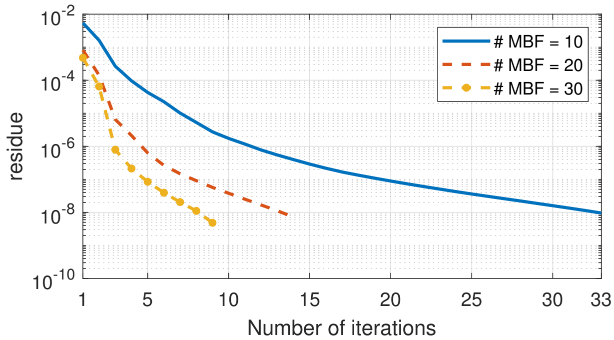

Fig. 9: Convergence of the proposed GMRES-MBF technique. A larger set of MBFs leads to a smaller number of iterations.

When the number of MBFs increases, more degrees of freedom are available to approximate the solution, which leads to a reduced number of iterations. Note that a higher number of MBFs also gives a better approximation of the solution at the first iteration. A faster convergence rate is obtained at the price of a larger required memory space, since $\mathbf{A}'$ has a size $(MP \times MP)$.

Table I summarizes the time required for this example, for three different number of MBFs. Those computation have been carried out on a Intel® i7-4790 CPU with 32GB of RAM. The preparation time (*tPrep*) includes the computation of the self impedance term, the computation of the patterns $\mathbf{p}$, the translation matrix $\mathbf{T}$, and the preconditioning (block-diagonal preconditioner was used in this example). The preparation time does not depend on the number of MBFs kept.

For each GMRES iteration, *tProduct* is the computational time of each of the two performed matrix-vector products (one computes the new generating vector, the second one computes the residue), *tFill* is the time required for filling $\mathbf{A}'$ (accelerated with FMM) and *tSolving* corresponds to solution of (3). The total computational time for different number of MBFs is computed as :

$$tTotal = tPrep + N_{iter}(2tProduct + tFill + tSolving) \quad (6)$$

Regarding the memory requirements, the patterns, the translation matrix and the self impedance block require 155 MB of RAM. $\mathbf{A}'$ is stored using 400 MB, 1.6 GB and 3.6 GB for 10, 20 and 30 MBFs respectively. One can notice that between 10 and 30 MBFs, the time needed to fill the MBF matrix and solve for the MBF coefficients is significantly smaller. Nevertheless, the number of iterations is higher, leading to an higher total computational time. On the other hand, less memory is required. A trade-off between time and memory has to made through the selection of a right number of MBFs, espically when dealing with denser arrays.

Those

V. Conclusion

We proposed a metallic element for phased arrays devoted to satellite-based SAR observation. The element does not truly have a very wide pattern, with a directivity as large as 8.5 dB. This may actually be favorable if the scan domain lies well within the main beam of the element pattern. For sparse arrays, as considered here, this may help restoring the aperture efficiency. The numerical analysis of such sparse arrays is made more efficient by selecting common MBFs for all elements, which reduces to a negligible quantity the time needed for pattern computation in the fast-multipole process. Further investigation will be needed in three areas: (i) co-designing the radiating element, and its embedded pattern, with the scan range of the array, (ii) efficiently including the effects on the radiation pattern of finite ground-plane [14] or satellite platform, (iii) optimizing the positions of the elements [15], while still accounting for the effects of mutual coupling.

Acknowledgment

This research has been supported by FRIA grant from the Belgium FNRS fund.

References

[1] D. J. Bekers, *et al.*, "Design of a Ka-band sparse array antenna for spaceborne SAR applications," in *47th Eur. Microw. Conf. (EuMC),* Nuremberg, Germany, 2017.

[2] C. Luison, *et al.*, "Aperiodic Arrays for Spaceborne SAR Applications," in *IEEE Trans. Antennas Propag.,* vol. 60, no. 5, pp. 2285-2294, May 2012.

[3] P. Capece, "Active SAR Antennas: Design, Development and Current Programs," in *Int. J. Antennas Propag.,* vol. 2009, 2009.

[4] S. Barbarossa and G. Levrini, "An antenna pattern synthesis technique for spaceborne SAR performance optimization," in *IEEE Trans. Geosci. Remote Sens.,* vol. 29, no. 2, pp. 254-259, Mar. 1991.

[5] C. Craeye and D. Gonzalez-Ovejero, "A review on array mutual coupling analysis," *Radio Science*, Vol. 46, Apr. 2011.

[6] E. Suter and J. R. Mosig, "A subdomain multilevel approach for the efficient MOM analysis of large planar antennas," in *Microwave Opt. Technol. Lett.,* Vol. 26, pp. 270-277, 2000.

[7] R. Coifman, V. Rokhlin and S. Wandzura, "The fast multipole method for the wave equation: A pedestrian prescription," in *IEEE Antennas Propag. Mag.,* Vol. 35, pp. 7-12, 1993.

[8] S. M. Rao, D. R. Wilton and A. W. Glisson, "Electromagnetic scattering by surfaces of arbitrary shape," in *IEEE Trans. Antennas Propag.,* Vol. 30, pp. 409-418, May 1982.

[9] Y. Saad and M. H. Schultz, "GMRES: A generalized minimal residual algorithm for solving nonsymmetric linear systems," in *SIAM J. Sci. Stat. Comput.*, Vol. 7, No. 3, pp. 856-869, Jul. 1986.

[10] O. A. Iupikov, *et al.*, "Domain-decomposition approach to Krylov subspace iteration," in *IEEE AWPL,* Vol. 15, 2016.

[11] R. Coifman, V. Rokhlin and S. Wandzura, "The fast multipole method for the wave equation: A pedestrian prescription, in *IEEE Antennas Propag. Mag.,* Vol. 35, pp. 712, 1993.

[12] H. Bui-Van, T. Pairon and C. Craeye, "Fast iterative techniques for the simulation of large antenna arrays," in *Proc. ICEAA 2018 Conf.,* Cartagena de Indias, Colombia, 2018.

[13] D. J. Ludick, *et al.*, "The CBFM-Enhanced Jacobi method for efficient finite antenna array analysis," in *IEEE AWPL*, Vol. 16, pp. 2700-2703, 2017.

[14] J. Cavillot, H. Bui Van and C. Craeye, "Efficient analysis of a 3D antenna installed on a finite ground plane," in *Proc. EuCAP 2018 Conf.*, London, Apr. 2018.

[15] O. Bucci, *et al.*, "Deterministic synthesis of uniform amplitude sparse arrays via new density taper techniques," *IEEE Trans. Antennas Propag.,* Vol. 58, pp. 1949-1958, Jun. 2010.